inorganics

MDPI

Article

Combining a Low Valent Molybdenum(0) Center with a Strongly σ-Donating Mesoionic Carbene Chelate Ligand—Synthesis and Structural Characterization

Benedict Josua Elvers *, Paul Schulan, Sebastian Pätsch, Christian Fischer and Carola Schulzke

Bioinorganic Chemistry, Institute of Biochemistry, University of Greifswald, Felix-Hausdorff-Str. 4, 17489 Greifswald, Germany

* Correspondence: benedict.elvers@uni-greifswald.de

Abstract: Triazolylidene ligands belong to a class of N-heterocyclic carbenes of growing chemical interest. Their precursors are readily available using Click chemistry and, therefore, highly modular for tuning their electronic characteristics. Due to their notable donor properties, these ligands are particularly suitable for modulating the electronic properties of the central ions of their complexes. Here, a bidentate bistriazolylidene which is a particularly strong donor ligand is combined with a low valent molybdenum(0) center and four carbon monoxide molecules as co-ligands. The novel complex exhibits characteristic electrochemical and IR-spectroscopic behavior. An X-ray structural analysis provides metrical details which are not entirely in agreement with spectroscopic data, likely going back to crystal packing effects. In comparison with precursor and ligand SCXRD data, notable geometrical changes induced by the coordination of the ligand to the metal can be observed. The analyses strongly support the bistriazolylidene ligand as being a particularly good donor of electron density towards the central metal. Potentially, these findings may support, in the future, the design of potent catalysts for the reductive activation of small molecules.

Keywords: click chemistry; molybdenum complexes; N-heterocyclic carbenes; mesoionic carbenes; bistriazolylidene ligands

Citation: Elvers, B.J.; Schulan, P.; Pätsch, S.; Fischer, C.; Schulzke, C. Combining a Low Valent Molybdenum(0) Center with a Strongly σ-Donating Mesoionic Carbene Chelate Ligand—Synthesis and Structural Characterization. *Inorganics* **2022**, *10*, 216. https://doi.org/10.3390/inorganics10110216

Academic Editors: Kostiantyn Marichev and Alejandro Bugarin

Received: 31 October 2022
Accepted: 18 November 2022
Published: 20 November 2022

1. Introduction

Click chemistry and its application in bio-orthogonal chemistry were recently honored with the Nobel prize, highlighting their outstanding chemical and biological importance [1–3]. The archetype of a Click reaction is the coupling of an azide with an alkyne to form a triazole [1,2,4]. Depending on the reaction conditions, either a 1,4- or a 1,5-regioisomer can be obtained. The former is realized using a copper catalyst (copper(I)-catalyzed azide-alkyne cycloaddition = CuAAC) while the use of ruthenium or bases results in the formation of the latter [4–7].

Triazoles have become important and frequently used tools in modern coordination chemistry. Both regioisomers exhibit diverse coordination sites before and after deprotonation of the acidic C-H bond in the heterocycle (resulting in a triazolide ligand) [8]. Triazoles can further be alkylated at a nitrogen position (preferably at N3) to yield triazolium salts [9]. The triazolium salts conserve the acidity of the C-H moiety in the heterocycle and yield triazolylidenes upon deprotonation [8,9]. Triazolylidenes are, for obvious reasons, more commonly called mesoionic carbenes (MICs) since no localized structure of these compounds can be drawn without showing a charge separation [10]. An overview of the structures of N-heterocyclic carbenes with a C-centered coordination site and the triazole and triazolium precursors is shown in Figure 1.

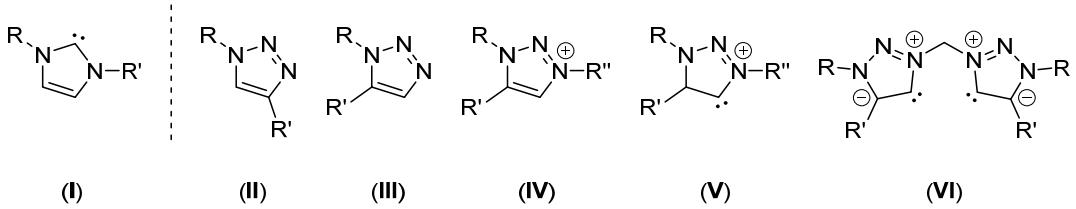

Figure 1. Triazole derived precursors and N-heterocyclic carbene (NHC). The well-known imidazole-2-ylidene (**I**) is shown for comparison reasons. 1,4-triazole (**II**) is obtained with a CuAAC; 1,5-triazole (**III**) is obtained in a base or Ru-catalyzed combination of azide (R) and alkyne (R′). N-alkylation (R″) of the 1,5-triazole yields the triazolium salt (**IV**) which is transformed by deprotonation to 1,2,3-triazol-4-ylidene (**V**). Using a bridging alkylation agent, a bis-1,2,3-triazol-4-ylidene (**VI**) can be obtained [8,11,12].

A major advantage of triazole-based ligands is that both N- and C-centered coordination sites are available [8] Another benefit is their easy steric and electronic modulation based on the Click syntheses [9]. Therefore, these ligands are already highly valued by coordination chemists. In particular, MICs of the 1,2,3-triazol-5-ylidene and 1,2,3-triazol-4-ylidene type have come into focus, as these ligands exhibit exceptional donor properties [10]. Their very strong donating nature renders them attractive co-ligands for (redox-switchable) catalysis [13–15], small molecule activation [16–19] and photochemistry [20–24].

However, only a few bidentate triazole-based MIC-containing ligands have been described in the literature so far [8,10,25,26]. One prominent example is 'i-bitz' which is often compared to 2,2′-bipyridine and its congeners due its topology [27]. Complexes featuring the i-bitz ligand were reported, for example, with manganese in the application of the catalytic oxidation of alcohols [28,29], with iron in the context of photoluminescence [21] and also with ruthenium and iridium [30–32]. Furthermore, different types of mixed ligands can be found in the literature. One example contains a triazolylidene as well as an imidazole-2-ylidene moiety which can be used in hydrogenation reactions [33]. A very interesting mixed bidentate MIC belongs to the pyridyl-mesoionic carbene (PyMIC) ligand class [34]. This class and their respective metal complexes were studied, for example, as electrocatalysts for the reduction in CO_2 [18], the formation of H_2 [17], the oxidation of water [35], in catalytic alcohol oxidation as well as ketone transfer hydrogenation [36] and as potential photosensitizers [34,37,38]. Furthermore, a particularly interesting anionic bidentate MIC ligand with a borane backbone was recently introduced and coordinated to cobalt [39].

One ligand with a notable bistriazolylidene binding motif (**VI**) has received surprisingly little attention so far (Figure 1) [11,40]. Aside its strong donating nature, this ligand exhibits a specific coordination motif that implies it being suitable for combinations with molybdenum. Complexes of molybdenum are of particular interest with respect to their use in small molecule activation. Thus, molybdenum phosphane complexes, as well as their NHC complexes, are already being investigated for their potential or actual ability to activate molecular nitrogen [41,42].

However, to date bistriazolylidene molybdenum complexes appear entirely elusive, despite such combination bearing considerable potential. As a first step towards such species, we decided to react a known bistriazolylidene with a carbonyl molybdenum precursor, expecting the resultant complex to retain some of its CO ligands. These ligands with their π-acceptor property are excellent reporter groups for the influence of the bidentate co-ligand on the electronic structure of the complex [43,44]. The molecular structures of the triazole precursor, the bistriazolium salt, and the successfully synthesized triazolylidene coordinated molybdenum complex obtained in this work—the first of its kind—provide a detailed insight into the notable changes in the ligand backbone upon coordination. These studies are complemented with infrared spectroscopic and electrochemical analyses, which confirm the remarkably strong donation of electron density by the investigated ligand.

2. Results and Discussion

2.1. Synthesis of the Target Compounds

Coupling azides and alkynes in a Click reaction facilitates introducing a variety of substituents, which in turn can influence the electronic structure of the subsequent ligand. In the context of this work, comparably simple alkyne and azide with phenyl substituents were chosen, due to the lower steric bulk compared to, e.g., tert-butyl groups and the comparably safer synthesis of the in-situ prepared azide [5].

The synthesis of the ligand used in this work was initially reported by the group of Sarkar [11]. The alkyne and the in-situ prepared azide are converted into the corresponding 1,5-triazole in a base-catalyzed cycloaddition (Scheme 1) [5]. A bridging methylene group is introduced between two triazoles using in-situ prepared methylene triflate (Scheme 1) in order to obtain the desired triazolium salt (**2**) [11].

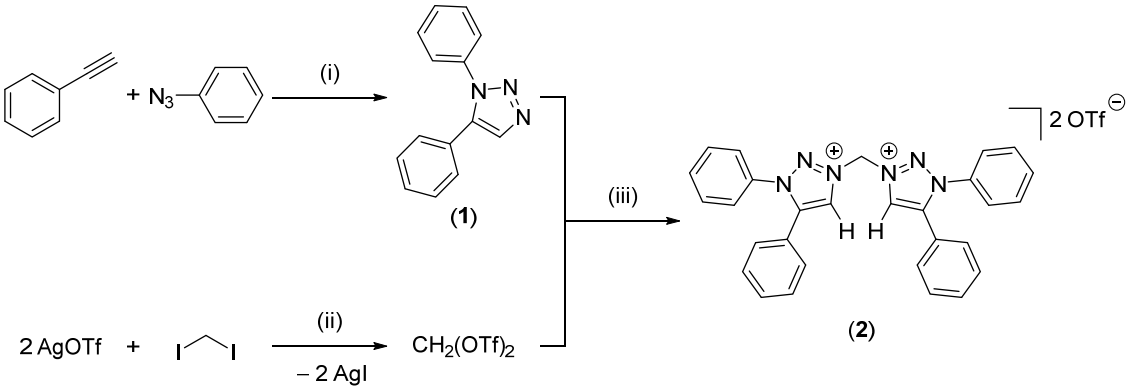

Scheme 1. Reaction scheme for the known syntheses of 1,5-diphenyl-1*H*-1,2,3-triazole (**1**) and 3,3′-methylenebis(1,5-diphenyl-1*H*-1,2,3-triazol-3-ium) triflate (**2**). (i): KOH, abs. DMSO. (ii): RT, n-hexane, dark. (iii): Reflux, mixed toluene/n-hexane, dark [5,11].

During the synthesis of 3,3′-methylenebis(1,5-diphenyl-1*H*-1,2,3-triazol-3-ium) triflate (**2**), crystals of the triazole (**1**) and the triazolium salt (**2**) were obtained. This offered the opportunity to directly analyse the structural changes upon alkylation and eventually upon coordination (vide infra).

The transition metal coordination of the chelating bistriazolylidene ligand (bta) used in this work was already published for ruthenium and copper centers [11,40,45]. However, a coordination with molybdenum has not been reported as of yet, while such combination might lead to a novel chemical platform in the context of small molecule activation, especially of dinitrogen [41,42].

To enforce the coordination of the chosen bistriazolylidene ligand, various reaction conditions and procedures were tested, and reaction progress monitored by a thin layer chromatography. A deprotonation strategy using strong bases such as potassium hydride, potassium bis(trimethylsilyl)amide (KHMDS) or N-isopropylamine (DIPEA) and subsequent in-situ coordination with preactivated complexes such as $[Mo(CO)_5(thf)]$, $[Mo(CO)_4(MeCN)_2]$ or $[Mo(CO)_4(piperidine)_2]$ proved unsuccessful [46–49]. Neither the isolation of the free carbene prior to coordination nor the isolation of its trapped selenone form for characterization purposes was possible. However, coordination could be achieved by i) following a literature known transmetalation reaction from an in-situ prepared silver complex (Scheme 2a) [50] or (ii)) using a metal complex with basic and labile ligands (Scheme 2b). The latter is essentially an adaptation of the use of basic metal precursors such as $Pd(OAc)_2$ or $[Pd(acac)_2]$ reported throughout the literature [51–54].

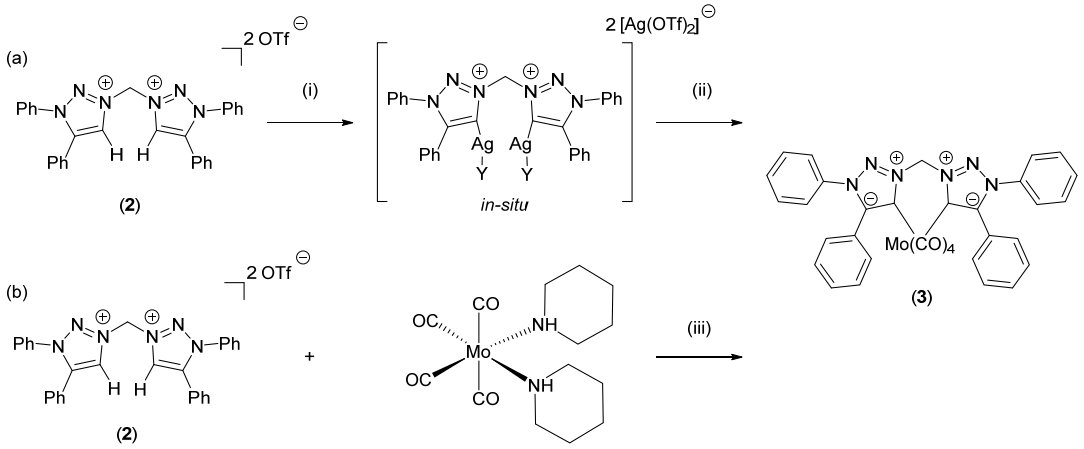

Scheme 2. Syntheses of $[Mo(CO)_4(bta)]$ (**3**) inspired by procedures in the literature through (**a**) a transmetalation reaction from silver or (**b**) using a metal complex with basic leaving groups in a one-pot reaction [10,11,55] (i): Ag_2O, LiCl, dark, Y = Cl or bta [55]; (ii): $[Mo(CO)_4(piperidine)]$; (iii): thf, 60 °C, 6 days.

In the one-pot reaction (Scheme 2b), the piperidine of $[Mo(CO)_4(piperidine)_2]$ successfully serves as a base for the deprotonation of the triazolium salt under reflux conditions in thf, as evidenced by obtaining colorless crystals of the piperidinium triflate [56] from the reaction mixture (Figure S2). The use of solvents with a higher boiling point such as acetonitrile or toluene or the use of thf at room temperature did not yield the target complex. Further purification using column chromatography is necessary to obtain (**3**) as a pure compound resulting in a yield of only ca. 10% at best. The low yield complicates subsequent analyses and renders reactivity studies with the complex nearly impossible. Fortunately, crystals of the target complex (**3**) could be obtained, which at least facilitates analysis.

2.2. X-ray Crystallography

Through repeated crystallization experiments, the molecular structures of the triazole (**1**), the triazolylidene precursor (triazolium salt) (**2**), and the molybdenum carbonyl complex coordinated by the bistriazolylidene (**3**) were eventually obtained. The molecular structures of all targeted compounds are shown in Figure 2. A summary of the most important metrical parameters with regard to the ligand backbone are provided in Table 1.

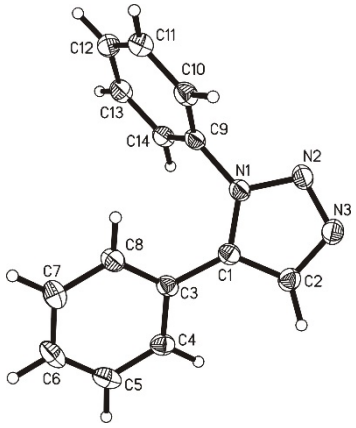

(**1**)

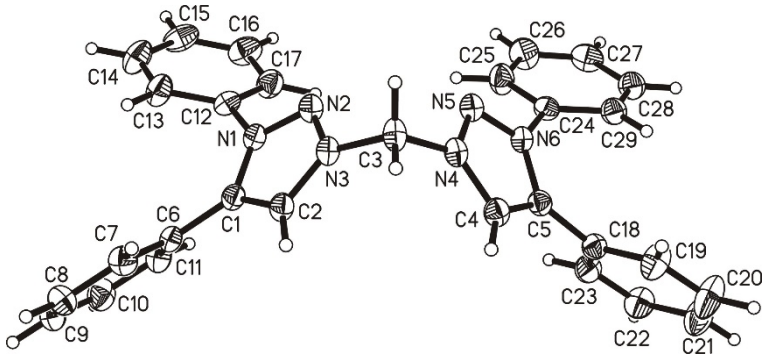

(**2**)

Figure 2. *Cont.*

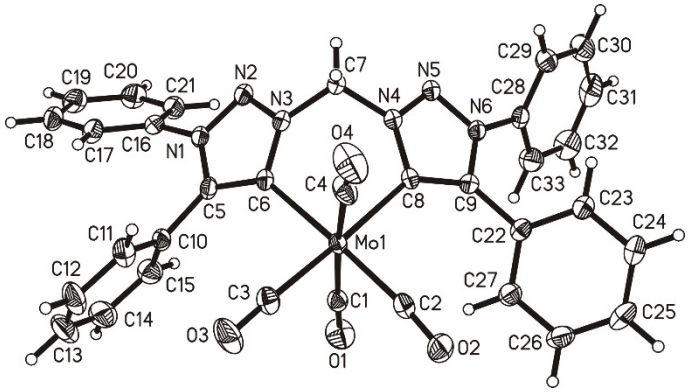

(**3**)

Figure 2. Molecular structure of 1,5-diphenyl-1H-1,2,3-triazole ((**1**); R = 2.93%, R_{int} = 3.79%), 3,3′-methylenebis(1,5-diphenyl-1H-1,2,3-triazol-3-ium) triflate ((**2**); R = 4.24%, R_{int} = 8.66%), and $[Mo(CO)_4(bta)]$ (**3**); R = 3.05%, R_{int} = 5.23%). In case of (**2**), the two triflate counter ions and in case of (**3**), a co-crystallized CH_2Cl_2 are omitted for clarity reasons. Ellipsoids are shown at the 50% probability level.

Table 1. Selected bond lengths (Å) and angles (°) of triazole (**1**), bistriazolium salt (**2**) and the bistriazolylidene backbone in $[Mo(CO)_4(bta)]$ (**3**).

Bond Label	(1)	(2)	Bond Label	(3)
N1-N2	1.3554(18)	1.322(2)	N1-N2	1.320(4)
N2-N3	1.3127(19)	1.318(2)	N2-N3	1.336(4)
N1-C1	1.362(2)	1.373(3)	N1-C5	1.369(5)
N3-C2	1.356(2)	1.347(3)	N3-C6	1.366(5)
N3-C3	-	1.463(2)	N3-C7	1.448(4)
C2-H2	0.98(3)	0.93(2)	C6-Mo	2.276(4)
C1-C2	1.375(2)	1.364(3)	C5-C6	1.392(5)
N5-N6	-	1.322(2)	N5-N6	1.321(4)
N4-C4	-	1.347(3)	N4-C8	1.366(5)
C4-H4	-	0.90(2)	C8-Mo	2.284(3)
N1-N2-N3	106.80(13)	103.70(15)	N1-N2-N3	101.5(3)
N4-N5-N6	-	103.29(16)	N6-N5-N4	101.6(2)
N3-C2-C1	109.27(14)	105.88(18)	N3-C6-C5	100.5(3)
N4-C4-C5	-	105.71(18)	N4-C8-C9	100.2(3)
N3-C2-H2	123.0(15)	123.6(13)	N3-C6-Mo	120.8(2)
N4-C4-H4	-	121.2(14)	N4-C8-Mo	120.5(2)
C1-C2-H2	127.8(15)	130.5(13)	C5-C6-Mo	137.2(3)
C5-C4-H4	-	133.1(15)	C9-C8-Mo	138.7(3)
N3-C3-N4	-	108.98(16)	N3-C7-N4	109.0(3)
C2-C3-C4	-	104.31(2)	C6-C7-C8	74.751(13)

Colorless crystals of 1,5-diphenyl-1*H*-1,2,3-triazole (**1**) were obtained upon layering a thf solution with *n*-hexane and slow evaporation. A structural comparison between the as of yet unknown molecular structure of (**1**) and the already published one of its protonated form [57] (Figure S1) reveals only minor differences. The protonated triazole has a slightly less acute N2-N3-C2 angle ((**1**): 109.19(13)u° vs. (**1**)H^+: 113.51°) and a slightly shortened N3-C2 bonding distance ((**1**): 1.356(2) Å vs. (**1**)H^+: 1.342 Å) [57]. Furthermore, the C1-C2 distances slightly decrease upon alkylation when transforming **1** to **2** ((**1**): 1.375(2) Å vs. (**2**): 1.364(3) Å), which is consistent with a more localized double bond character in the triazolium salt (**2**).

Crystals of 3,3′-methylenebis(1,5-diphenyl-1*H*-1,2,3-triazol-3-ium) triflate (**2**) were obtained by slow evaporation from acetone. Although bistriazolylidene ligands bridged by methylene groups have already been reported, no respective molecular structures of their salts are currently deposited in the CSD [11,40,45,58,59]. With the molecular structure of **2** we therefore provide the first one of such a ligand precursor. The most striking changes after introducing the bridging alkylation are shortened N1-N2/N5-N6 ((**1**): 1.3554(18) Å vs. (**2**): 1.322(2) Å), N1-C1/N4-C4 ((**1**): 1.362(2) Å vs. (**2**): 1.347(3) Å) and C2-H2/C4-H4 ((**1**): 0.98(3) Å vs. (**2**): 0.93(2)/0.90(2) Å) bond lengths. Assessing the latter is only possible because the respective hydrogen atoms could be refined freely, and this implies a decrease in C-H acidity as a result of the introduced charge and concomitant electron density compensation on the adjacent nitrogen atom.

Upon deprotonation and subsequent coordination with molybdenum, some essential changes in the bond distances and angles occur. For clarity reasons, only the changes in one side of the triazole ring will be discussed in detail; they are mirrored in the opposite side. [Mo(CO)$_4$(bta)] (**3**) crystallizes in the monoclinic space group $P2_1$ with two molecules per unit cell. The C1-C2 ((**2**): 1.364(3) Å vs. (**3**): C5-C6: 1.392(5) Å) and N3-C2 ((**2**): 1.347(3) Å vs. (**3**): N3-C6: 1.366(5) Å) bond distances of the former bistriazolium compound become longer upon coordination while the N3-C2-C1 angle is now more acute ((**2**): 105.88(18)° vs. (**3**): N3-C6-C5: 100.5(3)°). This finding is in line with an elevated s-orbital contribution of the carbene lone pair [8,60,61] Additionally, the N2-N3 ((**2**): 1.318(2) Å vs. (**3**): 1.36(4) Å) and N3-C3 ((**2**): 1.347(3) Å vs. (**3**): N3-C6: 1.366(5) Å) distances are slightly increased which possibly indicates a more delocalized system following the same trend as in the comparison of the triazole (**1**) and its bistriazolium salt (**2**) (vide supra).

The change in the angle spanned by the coordinating carbon atoms through the bridging methylene carbon is particularly striking. While the bistriazolium salt (**2**) exhibits a backbone angle (C2-C3-C4) of 104.31(2)°, the triazolylidene ligand in complex (**3**) has a significantly smaller one (C6-C7-C8) of 74.751(13)°. This difference is particularly evident in the superposition of the structures in Figure 3.

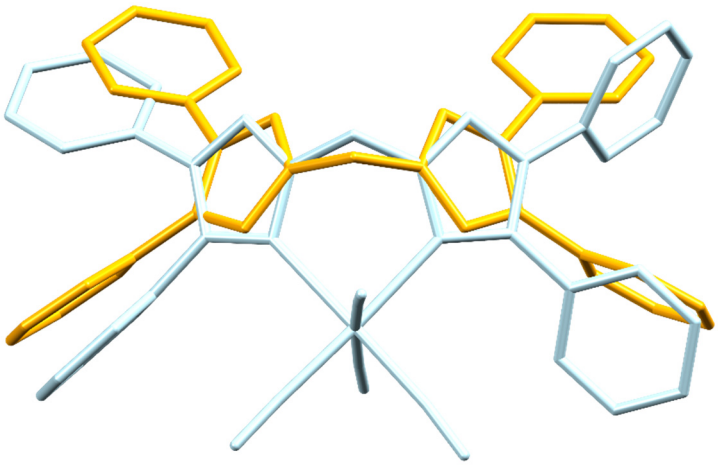

Figure 3. Structural overlay of the bistriazolium salt (**2**) and its corresponding bistriazolylidene complex (**3**). The counterion of (**2**) and the co-crystallized solvent of (**3**) are not shown for clarity reasons.

Changing the angle of the ligand backbone in a butterfly kind of motion is necessary to ensure optimal bidentate coordination of the carbene ligand. This finding is accompanied by a N1-N2-N3 angle which is slightly more acute ((**2**): 103.70(15)° vs. (**3**): 101.5(3)°), while the N3-C3/7-N4 angle remains almost unaffected ((**2**): 108.98(16)° vs. (**3**): 109.0(3)°). The changes caused by ligand coordination are shown schematically in Figure 4.

In the literature, MICs are described as exceptionally strong donor ligands [8,10,26]. This can be, and was, quantified for monodentate ligands, while the methods described are not directly applicable to chelating ligands and for the respective analyses of the latter no

standardized method has been introduced to date [10]. In order to relatively quantify the donor strength of NHCs in complexes, co-ligand carbon monoxide is a suitable reporter as already demonstrated for other carbonyl complexes [27,33,62]. Provided electron density from a ligand can be transferred via the metal and orbitals of suitable symmetry to the CO ligands [44]. Due to their π-backbonding ability, coordination with metal centers results in a weakening of the C≡O bond strength and, hence, in an increased C≡O distance, which is the more pronounced the richer in electron density the metal centers are (resulting also in shorter metal to carbonyl-carbon bonds). For a comparison of the respective metrical parameters of this work's complex with others, a number of suitable tetracarbonyl molybdenum complexes were selected from the CSD. Aside from the very well-characterized dppe and bipy complexes, those with a similar bite geometry and at least one bound carbene were chosen, as well as the only as of yet structurally characterized tetracarbonyl molybdenum complex with a MIC ligand (PyMIC). The data for the bta coordinated complex (**3**) and these selected examples are summarized in Table 2.

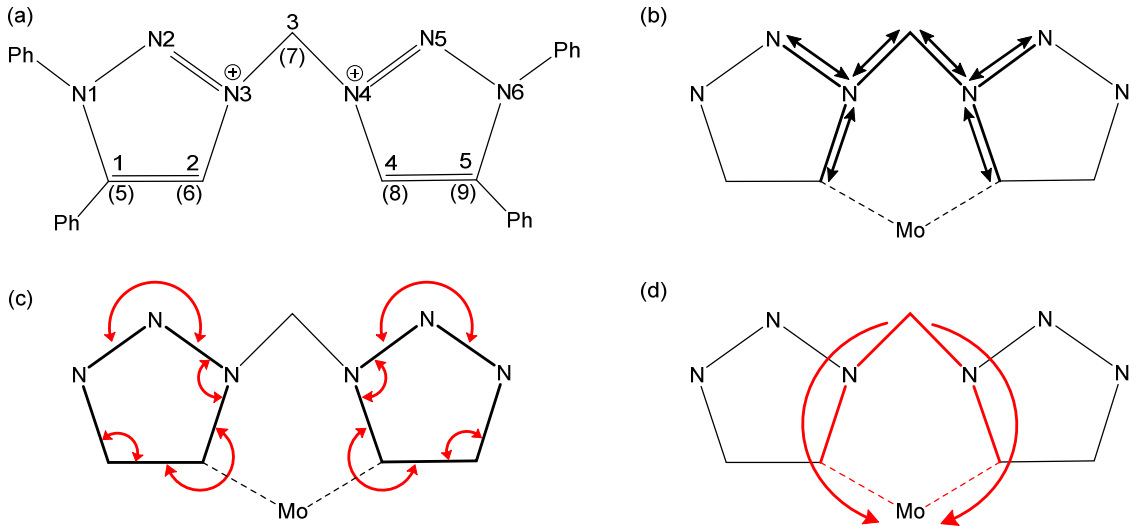

Figure 4. Schematic representation of the observed changes in bond distances (black arrows) and angles (red arrows) of the bistriazolium (**2**) and the molybdenum coordinated bistriazolylidene (**3**) moieties. (**a**): Labels of the bistriazolium and the coordinated bistriazolylidene (in brackets, where deviating). (**b**): significantly shortened bond lengths after coordination. (**c**): significantly changed angles. (**d**): Changes in the torsion angle in a butterfly kind of motion through coordination with molybdenum.

The M-$C_{carbene}$ distances in **3** are with 2.276(4) Å and 2.284(3) Å comparable to those of other carbene-coordinated complexes (Table 2). A short Mo-CO distance with a simultaneously elongated C≡O bond indicates an increased donor strength of the non-carbonyl ligand (vide supra). This impact is, naturally, more significant for the carbonyl ligands *trans* to the respective donor atoms (in Table 2 defined as $CO_{eq.}$). For those, only the bipy-coordinated complex exhibits an even shorter Mo-CO_{eq} bond compared to **3**. The observed C-$O_{eq.}$ distances are in accordance with that; i.e., $[Mo(CO)_4(bipy)]$ has the longest $CO_{eq.}$ and $CO_{ax.}$ bonds of all. This is, to some extent, surprising because triazolylidene ligands were declared the stronger donors [27]. Compared with the other complexes, no notable differences or consistent trends are found in the metrical parameters in Table 2. A fundamental problem with the direct comparison of bond distances from crystalline material is the possibility of non-canonical hydrogen bonds involving the CO ligands, which impacts the distribution of electron density. The structural packing patterns of bipy complex and **3** indeed show distinct hydrogen bonding networks (Figure S4). This must therefore be kept in mind when attempting to link structural metrical parameters to the apparent donor strength of the ligands used. The donor strength of the ligand and the

distribution of electron density is further related to the L-M-L bond angle, which affects the quality of orbital overlap between central metal and ligands [63]. The L-M-L bond angles of only the PyMIC and bipy coordinated complexes differ substantially from the average, which can be attributed to the steric constraints in the ligand backbones. The steric stress exerted by the coordinated ligand is in octahedral complexes reflected in the $CO_{ax.}$-M-$CO_{ax.}$ angle as its deviation from 180°. This angle for **3** is 172.77(19)°, which is a little more relaxed than in most of the compared complexes but not much different from the average. It suggests only insignificant spatial strain from the bidentate ligand, if any.

Table 2. Selected bond distances (Å) and angles (°) of the bistriazolylidene coordinated complex (**3**) and selected examples for [Mo(CO)$_4$(LˆL)] complexes from the literature.

LˆL=	**bta**	**I_{et}ˆI_{et}**	**bI_{et}ˆbI_{et}**	**$(I_{me})_2$** [a]	**PyMIC**	**dppe**	**bipy**
Ref.	This Work	[64]	[65]	[66]	[67]	[68]	[69]
Mo-L1	2.276(4)	2.261(4)	2.249(2)	2.293(3)	2.202(1)	2.500(2)	2.249(3)
Mo-L2	2.284(3)	2.259(4)	2.257(2)	2.293(3)	2.275(1)	2.495(2)	2.240(3)
Mo-$CO_{ax.}$	2.030(4)	2.036(6)	2.041(3)	2.032(3)	2.051(2)	2.053(9)	2.056(4)
	2.018(3)	2.024(6)	2.031(3)	2.024(3)	2.040(2)	2.030(9)	2.023(4)
Mo-$CO_{eq.}$	1.986(3)	1.988(5)	2.000(3)	1.981(3)	1.997(2)	1.999(8)	1.962(4)
	1.961(4)	1.977(6)	1.986(3)	1.979(3)	1.973(1)	1.974(8)	1.952(4)
C-$O_{ax.}$	1.146(5)	1.143(6)	1.143(3)	1.146(4)	1.149(2)	1.143(9)	1.150(4)
	1.142(4)	1.134(6)	1.137(4)	1.144(4)	1.146(29	1.120(9)	1.134(4)
C-$O_{eq.}$	1.156(5)	1.157(6)	1.150(3)	1.157(3)	1.158(2)	1.164(9)	1.168(4)
	1.152(4)	1.149(6)	1.145(4)	1.156(3)	1.156(2)	1.140(8)	1.160(4)
L1-Mo-L2	83.60(14)	79.6(2)	80.37(9)	85.64(10)	72.83(4)	80.2(1)	72.36(10)
L1-Mo-CO	175.54(15)	173.3(2)	175.49(11)	178.98(10)	168.22(5)	171.4(2)	171.37(12)
L2-Mo-CO	177.4(2)	175.1(2)	176.01(10)	178.50(10)	169.71(5)	170.6(6)	170.66(12)
$CO_{ax.}$-Mo-$CO_{ax.}$	172.77(19)	170.2(2)	170.42(10)	169.82(11)	171.77(6)	176.6(3)	167.83(13)

[a]: coordinated by two monodentate ligands; L1, L2 = non-carbonyl donor atoms; ax.: axial, i.e., perpendicular to L1, L2; eq.: equatorial, i.e., in-plane with L1, L2; I_{et}ˆI_{et} = bis(3-ethyl-2,3-dihydro-1*H*-imidazol-2-ylidene)methane [64], bI_{et}ˆbI_{et} = bis(3-ethyl-2,3-dihydro-1*H*-benzoimidazol-2-ylidene)methane [65], $(I_{me})_2$ = 2x 1,3-dimethyl-imidazol-2-yliden [66], PyMIC = 5-(2,6-diisopropylphenyl)-1-methyl-3-(pyridin)-triazo-2-ylidene [67], dppe = 1,2-bis(diphenylphosphino)ethane [68], bipy = bipyridine [69]. For chemical structures of these ligands see Figure S3.

Since the evaluation of the ligands' donor abilities from structural metrical parameters is limited by intermolecular interactions in the crystal lattices further analytical methods need to be consulted for reaching a better justified judgement.

2.3. Spectroscopic Results

Infrared spectroscopy provides information on atom-to-atom distances and the strength of the bond between these atoms since the observed wavenumbers reflect the energy needed to excite respective molecular vibrations. Moreover, C≡O stretching vibrations appear in a region of the IR-spectral range, in which only very few moieties are observed. This method is, hence, perfectly suited to evaluate the impact of the carbene ligand on the carbonyl ligands via the metal center. For setting them into context, a comparison of C≡O stretching vibrations with complexes of the same principal structure is a suitable approach [43]. Complex **3** exhibits three signals in the IR spectrum at 1990 cm^{-1}, 1864 cm^{-1}, and 1810 cm^{-1} that can be clearly assigned to C≡O stretching vibrations. The signal at 1864 cm^{-1} is comparably broad, indicating a potential signal overlap. DFT calculations did indeed show that two theoretically computed signals are very close to each other (within 2 cm^{-1}, see Figure S18). The C≡O vibration wavenumbers of selected examples of octahedral carbonyl complexes bearing chelating ligands are listed in Table 3 (for chemical structures of ligands see Figure S3).

Table 3. Selected examples of CO stretching vibrations (in cm^{-1}) in the IR spectra of $Mo(CO)_4(L\hat{}L)$ complexes (L^L = chelating ligand).

L^L=	bta	I^I	$I_{et}\hat{}I_{et}$	$bI_{et}\hat{}bI_{et}$	$(I_{me})_2$	T^T	PyMIC	dppe	bipy	phen	pDAB
Ref.	This Work [a]	[70] [b]	[64] [c]	[65] [c]	[66] [b]	[70] [b]	[67] [d]	[49] [b]	[71] [e]	[72] [a]	[73] [f]
ν_1(CO)	1990	1994	1987	1994	1994	2005	2006	2018	2016	2010	2016
ν_2(CO)	1864	1872	1876	1875	1868	1884	1896	1923	1904	1915	1901
ν_3(CO)	1810	1841	1818	1860	1863	1853	1876	1896	1877	1875	1869
ν_4(CO)			1799	1817	1838		1830	1884	1832	1835	1832

Measured in/by [a]: KBr, [b]: thf, [c]: ATR, [d]: CH_2Cl_2, [e]: CH_3CN), [f]: Nujol. bta = bicarbene used for complex **3**, I^I = bis(3-methyl-2,3-dihydro-1*H*-imidazol-2-ylidene)methane [70], $I_{et}\hat{}I_{et}$ = bis(3-ethyl-2,3-dihydro-1*H*-imidazol-2-ylidene)methane [64], $bI_{et}\hat{}bI_{et}$ = bis(3-ethyl-2,3-dihydro-1*H*-benzoimidazol-2-ylidene)methane [65], $(I_{me})_2$ = 2x 1,3-dimethyl-imidazol-2-yliden [66], T^T = bis(4-methyl-4,5-dihydro-1*H*-1,2,4-triazol-2-ylidene)methane [70], PyMIC = 5-(2,6-diisopropylphenyl)-1-methyl-3-(pyridin)-triazo-2-ylidene [67], dppe = 1,2-bis(diphenylphosphino)ethane [49], bipy = bipyridine [71], phen = phenanthroline [72], pDAB = N,N′-bis(phenyl)diazaubutadiene [73].

Employing the MIC ligand bta in molybdenum complex **3** results in a particularly strong bathochromic shift of the CO stretching wavenumbers. A lower wavenumber for the C≡O stretching vibration indicates a significantly weakened C≡O bond, which derives from relatively stronger electron density donation to CO by the metal through π-backbonding (vide supra). This necessarily is modulated by the donor strength of the non-carbonyl co-ligand. $[Mo(CO)_4(bta)]$ (**3**) exhibits the second lowest C≡O stretching vibration energy of all compared complexes, with a wavenumber of 1810 cm^{-1}, only surpassed by the bidentate ligand with ethyl substituents on the two imidazol-2-ylidene donor moieties ($I_{et}\hat{}I_{et}$) at 1799 cm^{-1} [64]. The closely related bis(3-ethyl-2,3-dihydro-1H-imidazol-2-ylidene)methane (I^I) complex, on the other hand, has its lowest C≡O stretching vibration at 1841 cm^{-1} [70]. This implies that with a change in the substituent on the imidazol-2-ylidene from ethyl to methyl, a significant modulation of the donor strength of the carbene ligand might occur, while that of the MIC ligand in **3** lies in between those two. Using a benzimidazolylidene backbone ($bI_{et}\hat{}bI_{et}$) or two monodentate imidazol-2-ylidene ligands ($(I_{me})_2$) the lowest C≡O stretching vibrations are observed at 1817 cm^{-1} and 1838 cm^{-1}, respectively [65,66]. The molybdenum tetracarbonyl complex coordinated by the ditriazolin-3,3′-diylidene ligand (T^T) exhibits its lowest energy carbonyl vibration at 1853 cm^{-1}, indicative of being the weakest donor of electron density among all of the carbene ligands assessed [70,74]. The only other evaluated MIC bearing complex with the PyMIC ligand has its lowest carbonyl stretching vibration at 1830 cm^{-1}, suggesting that this ligand is a weaker donor compared to bta in **3** [67]. The phosphine (dppe) or imine (bipy, phen, pDAB) bearing complexes all require higher energy for the excitation of their CO stretching vibrations than **3** [49,72,73]. In summary, the MIC ligand bta in **3** exhibits superior donor strength ability compared to all but one of the complexes selected for comparison. Notably, this is for the bipy complex and for **3,** in particular in contrast to the crystallographic evaluation, emphasizing again that distinct evaluation methods must be applied to reach reliable conclusions.

2.4. Electrochemical Investigations

To further investigate the electronic characteristics of the bistriazolylidene complex (**3**), cyclic voltammetric studies were performed at different scan rates (Figure 5).

Complex ***3*** features one metal centered oxidation signal at $E_{\frac{1}{2}} = -0.125$ V vs. the ferrocene/ferrocenium couple (Fc/Fc^+) with $E_{pa} = -0.015$ V and $E_{pc} = -0.235$ V. DFT confirms that it is the metal which is being oxidized since the computed HOMO has predominant metal contribution (Figure S19). The comparably low value of −0.125 V vs. Fc/Fc^+ reflects relatively easier oxidation of the central metal, going back to the very good donating ability of the coordinated MIC ligand. The electrochemical oxidation and re-reduction in **3** appears to be at least chemically reversible, although the large difference in anodic

and cathodic potential ($U_{pa} - U_{pc}$ = 220 mV at 100 mV/s) suggests electrochemically only quasi-reversibility [75]. This rather typical behavior under cyclovoltammetric conditions has already been described for other carbonyl complexes [44].

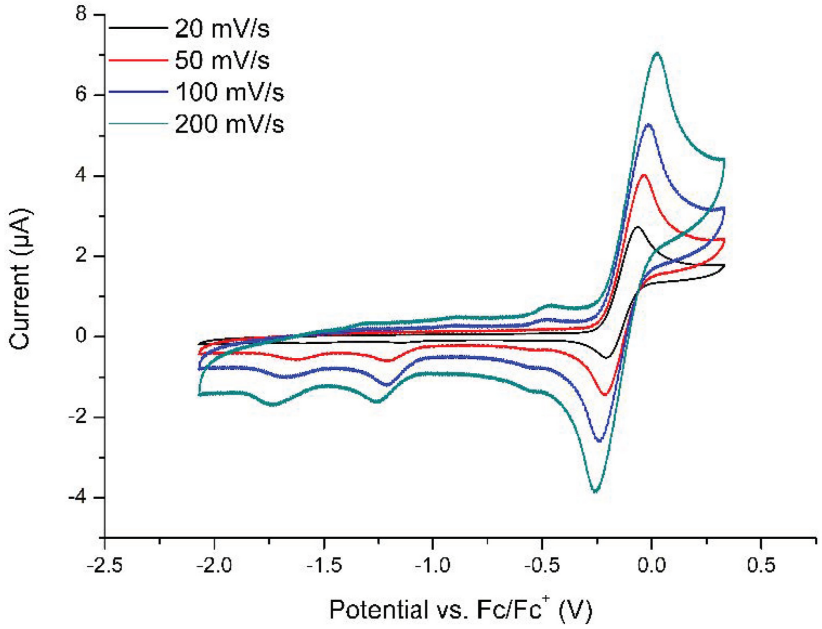

Figure 5. Cyclic voltammograms of **3** in CH_3CN using 0.1 M nBu_4NPF_6 as supporting electrolyte at different scan rates under an argon atmosphere measured at room temperature.

In contrast to $[Mo(CO)_4(PyMIC)]$, complex **3** exhibits a reversible oxidation signal and no further ligand centered reductions within the scan range of the used solvent/electrolyte system [67]. The oxidaiton signal of $[Mo(CO)_4(bta)]$ (**3**) $E_{\frac{1}{2}}$ = −0.125 V vs. Fc/Fc^+ is more negative compared to $[Mo(CO)_4(PyMIC)]$ featuring an E_{pa} at +0.08 V vs. Fc/Fc^+. This is in accordance with a superior donor strength of the bistriazolylidene ligand in complex **3** as already concluded from the IR spectroscopic data.

3. Materials and Methods

3.1. General Considerations

All anaerobic manipulations were carried out under argon using standard Schlenk line techniques. Anaerobic thf, toluene and *n*-hexane were freshly distilled from sodium/benzophenone prior to use. Anaerobic CH_2Cl_2 was dried using $CaCl_2$ and refluxed for several days prior to use. Anaerobic DMSO, $[Mo(CO)_6]$ and methylene iodide were bought from commercial sources. $[Mo(CO)_4(piperidine)]$ was prepared according to the literature [47].

Elemental analyses (C, H, N, and S) were carried out with an Elementar Vario MICRO elemental analyzer. IR spectra were recorded as KBr pellets with an FT-IR spectrometer Shimadzu IRAffinity-1. ^1H, ^{13}C, ^{31}P NMR spectra were recorded on a Bruker Avance II 300 spectrometer (300, 75 and 121.5 MHz, respectively). Chemical shifts (δ) are given in parts per million (ppm), using solvent signals or tetramethylsilane as reference. $CDCl_3$ ^1H: δ = 7.24 ppm; ^{13}C: δ = 77.0 ppm; acetone-d6 ^1H = 2.05 ppm; ^{13}C = 29.84 ppm; thf-d8 ^1H: δ = 1.72 ppm; ^{13}C: δ = 25.2 ppm) relative to external tetramethylsilane (δ = 0 ppm).

3.2. SCXRD

We mounted 1,5-Diphenyl-1*H*-1,2,3-triazole (1) on LithoLoops produced by Molecular Dimensions fixed on pins produced by Hampton Research. Data was recorded at 100 K on an XtaLAB Synergy diffractometer from Rigaku with a mirror monochromated Cu-Kα-radiation (λ = 1.54184 Å). As detector, a Hybrid Pixel Array Detector (HyPix) was

used. Moreover, 3,3′-Methylenebis(1,5-diphenyl-1H-1,2,3-triazol-3-ium) triflate (2) and [$Mo(CO)_4$(bta)] (3) were mounted on a glass fiber in inert paraffin oil. Data were recorded at 170 K on a STOE-IPDS 2T diffractometer with graphite-monochromated Mo-Kα-radiation (λ = 0.71073 Å). Absorption corrections were performed using X-Red32 and X-Shape (by STOE & Cie GmbH 2010) in case of the Mo source or CrysAlisPro 1.171.42.61a (Rigaku OD, 2022) in the case of the Cu source. All of the structures were solved by direct methods (SHELXS-2013 or SHELXT-2016) and refined by full-matrix least-squares techniques using the SHELXL executable and the WingX GUI [76–78]. All non-hydrogen-atoms were refined with anisotropic displacement parameters. Unless stated otherwise, all hydrogen atoms were refined isotropically at calculated positions using a riding model with their U_{iso} values constrained to 1.2 times U_{eq} of their pivot atoms for aromatic or to 1.5 times U_{eq} for all other carbon atoms. For 1, all hydrogen atoms were refined freely. For 2, all non-aromatic hydrogen atoms were refined freely. General crystallographic, crystal and refinement data for 1, 2 and 3 are provided in the supplementary data file (Tables S2–S4). Crystallographic data were deposited with the Cambridge Crystallographic Data Centre, CCDC, 12 Union Road, Cambridge CB21EZ, UK. These data can be obtained free of charge on quoting the depository numbers CCDC 2215829 (3), 2215830 (1), and 2215831 (2) by FAX (+44-1223-336-033), email (deposit@ccdc.cam.ac.uk) or their web interface (at http://www.ccdc.cam.ac.uk).

3.3. DFT Calculations

All density functional theory calculations were performed with the ORCA program package, version 4.1.2 [79]. The geometry was optimized starting from the crystal structure using the BP86 density functional under the resolution of the identity approximation [80–82]. Ahlrichs' triple-ζ basis set def2-TZVP with the effective core potentials for Mo was used, except for the carbon and hydrogen atoms where def2-SVP was employed [83,84]. As the auxiliary basis set, def2/J was chosen [85]. Dispersion corrections were included according to Grimme's D3zero scheme [86]. Tight SCF and optimization convergence criteria as well as a finely woven grid size of 7 (Lebedev quadrature) were chosen in the ORCA nomenclature. The integration accuracy parameter, which is used to calculate the number of radial shells considered, was set to 7.0. To confirm the geometries obtained as true minima on the potential energy surface, frequency calculations were run with the same setup as for the geometry optimizations except for the omission of the solvent model. From these calculations, the computed IR spectra and the thermodynamic data were extracted.

3.4. Synthetic Procedures

3.4.1. 1,5-Diphenyl-1H-1,2,3-triazole (**1**)

The multi-step preparation of 1,5-diphenyl-1*H*-1,2,3-triazole (**1**) follows the procedure described by Kwok et al. [5], applying a minor modification. In-situ prepared phenyl azide (10 g, 84 mmol, 1 eq.) was dissolved in 80 mL of anaerobic DMSO in a Schlenk flask and phenylacetylene (8.6 g, 84 mmol, 1 eq.) was added via syringe while freshly crushed potassium hydroxide (0.47 g; 0.008 mol; 0.1 eq.) was added as solid under an argon counter stream. After stirring for 2 h at room temperature, thin layer chromatography is performed to check for remaining azide. Upon completion of the reaction, the reaction mixture was added to 5000 mL H_2O and stirred for 1.5 h. The crude product was filtered using a G4 glass frit and washed excessively with water. After drying in vacuo, a recrystallization in ethyl acetate was carried out. Furthermore, 1,5-Diphenyl-1*H*-1,2,3-triazole (**1**) was obtained as white, microcrystalline needles. Crystals of **1** suitable for SCXRD were obtained upon recrystallization in a mixture of thf/*n*-hexane. Yield: 44% (8.24 g, 37 mol).

^{1}H NMR (300 MHz, $CDCl_3$): δ (ppm) = 7.19–7.26 (m, 2 H); 7.31–7.47 (m, 8 H); 7.87 (s, 1 H). ^{13}C NMR (300 MHz, $CDCl_3$): δ (ppm) = 125.2 ($CH_{arom.}$); 126.8 ($CH_{arom.}$); 128.6 ($CH_{arom.}$); 128.8 ($CH_{arom.}$); 129.2 ($CH_{arom.}$); 129.3 ($CH_{arom.}$); 133.4 ($CH_{arom.}$); 136.6 ($C_{quart.}$); 137.7 ($C_{quart.}$). DEPT-135 NMR (300 MHz, $CDCl_3$): δ (ppm) = 125.2 (pos., $CH_{arom.}$); 128.6 (pos., $CH_{arom.}$); 128.8 (pos., $CH_{arom.}$); 129.2 (pos., $CH_{arom.}$); 129.3 pos., $CH_{arom.}$); 133.4

(pos., $CH_{arom.}$). IR (KBr), ν (cm^{-1}) = 3124, 2020-1632, 1694 (N-C=C), 1595 (N=N), 1503 (C=C), 1227-860 ($CH_{arom., in\text{-}of\text{-}plane}$), 760-693 ($CH_{arom., out\text{-}of\text{-}plane}$). Rf-value (*n*-hexane): 0.87. Elemental analysis calculated for $C_{14}H_{11}N_3$: C: 75.98%; H: 5.01%, N: 18.99%. Found: C: 75.99% H: 5.01%, N: 18.99%.

3.4.2. Synthesis of 3,3′-Methylenebis(1,5-diphenyl-1H-1,2,3-triazol-3-ium) triflate (**2**)

We prepared 3,3′-Methylenebis(1,5-diphenyl-1*H* -1,2,3-triazol-3-ium) triflate (**2**) with minor modifications to the literature described method [11]. Methylene iodide (6.65 mg; 2.5 mmol; 1 eq.) is suspended in 10 mL of anaerobic *n*-hexane. AgOTf is placed in an evacuated three-necked flask which is protected from light. The methylene iodide-hexane solution is then added to AgOTf to obtain an off-white (or beige) slurry. This mixture is heated under anaerobic reflux condition and stirred for 6 h resulting in a brownish slurry. In a separate Schlenk flask, the triazole (1) (1.3422 g; 6.1 mmol; 2.5 eq.) is prepared as a solution in approximately 25 mL of anaerobic toluene. The mixture which is heated to reflux condition is filtered anaerobically onto **1** and the flask used is post-rinsed with 5 mL of anaerobic *n*-hexane. The combined reaction mixture refluxes anaerobically for another 6 h. After cooling, the flask's contents are added to 250 mL aerobic Et_2O. Finally, the transferred material is filtered using a G4 glass frit and washed twice with 50 mL Et_2O each. After drying in vacuo, the product was obtained as an air-stable fluffy white powder. Crystallization was achieved by dissolving **2** in acetone and slow evaporation of the solvent. Yield: 42.3% (957 mg, 1.27 mmol).

^{1}H NMR (300 MHz, acetone-d6): δ (ppm) = 7.47–7.82 (m, 20 H); 8.11 (s, 2 H); 9.69 (s, 2 H). ^{13}C NMR (300 MHz, acetone-d6): δ (ppm) = 65.9 (CH_2); 123.3 ($C_{quart.}$, phenyl); 127.4 ($CH_{arom.}$); 130.0 ($CH_{arom.}$); 130.9 ($CH_{arom.}$); 131.0 ($CH_{arom.}$); 132.2 ($CH_{arom.}$); 132.7 ($CH_{arom.}$); 133.4 ($CH_{arom.}$); 135.2 ($C_{quart.}$, heteroarom.); 145.7 ($CH_{arom.}$, heteroarom.). DEPT-135 NMR (300 MHz, acetone-d6): δ (ppm) = 65.9 (neg., CH_2); 127.4 (pos., $CH_{arom.}$); 130.0 (pos., $CH_{arom.}$); 130.9 (pos., $CH_{arom.}$); 131.0 (pos., $CH_{arom.}$); 132.2 (pos., $CH_{arom.}$); 132.7 (pos., $CH_{arom.}$); 133.4 (pos., $CH_{arom.}$); 145.7 (pos., $CH_{arom.}$). IR (KBr), ν (cm^{-1}) = 3074, 1860-1627, 1492 (C=C), 1151 ($CH_{arom., in\text{-}of\text{-}plane}$), 1032 ($CH_{arom., in\text{-}of\text{-}plane}$), 765-638 ($CH_{arom., out\text{-}of\text{-}plane}$). Rf-value (thf): 0.44.

3.4.3. Synthesis of $[Mo(CO)_4(bta)]$ (**3**)

For the synthesis of $[Mo(CO)_4(bta)]$ (**3**) two different synthetic routs (**A** & **B**) proved useful.

(A) Preparation of $[Mo(CO)_4(bta)]$ (**3**) by transmetalation with silver oxide

For the preparation of $[Mo(CO)_4(bta)]$ (**3**), 3,3′-methylenebis(1,5-diphenyl-1*H* -1,2,3-triazol-3-ium) triflate (**2**) (154.5 mg, 0.2 mmol, 1 eq.), Ag_2O (164.5 mg, 0.7 mmol, 3.5 eq.) and LiCl (86.81 mg, 2 mmol, 10 eq.) are placed in a darkened two-neck flask and evacuated. Subsequently, 10 mL of anaerobic CH_2Cl_2 is added to the reaction mixture. The white, milky mixture is stirred in the dark for two days. After two days, a color change to a cloudy brown occurs. $[Mo(CO)_4(piperidine)_2]$ (76.1 mg; 0.2 mmol; 1 eq.) is placed together with a stirring bar in a separate, darkened Schlenk flask and the crude brown mixture is anaerobically filtered onto this solid using a 0.2 µm syringe filter. The mixture is left to stir in the dark for six more days. The reaction progress was continuously monitored by thin layer chromatography with a focus on the intensity/size of the product spot. After six days, the stirring is stopped, and the mixture kept undisturbed until the formed AgCl settles. The supernatant solution is taken up with a syringe filter (0.2 µm) and filtered into a new Schlenk flask. The solvent is removed using a cold trap, leaving a red foam on the wall of the Schlenk flask. The product is further purified using aerobic column chromatography with *n*-hexane/thf 2:3. An anaerobic crystallization mixture is then prepared with the ratio *n*-hexane/thf 2:1 to obtain the product as red, prismatic crystals. Yield: 9.1% (12 mg, 0.018 mmol).

(B) Preparation of $[Mo(CO)_4(bta)]$ (**3**) in a one-pot synthesis using $[Mo(CO)_4(piperidine)_2]$ under reflux conditions

$[Mo(CO)_4(piperidine)_2]$ (75.9 mg, 0.21 mmol, 1 eq.) and 3,3′-methylenebis(1,5-diphenyl-1*H*-1,2,3-triazol-3-ium) triflate (**2**) (160.2 mg, 0.21 mmol, 1 eq.) are transferred to a pressure-stable Schlenk vessel, evacuated and refilled with an argon atmosphere. Upon the addition of 15 mL of anaerobic thf, the mixture was heated in an oil bath at 60 °C while vigorously stirring for four days. During the reaction, a color change from milky white to brownish-red was observed. The reaction progress was continuously monitored by thin layer chromatography with a focus on the intensity/size of the product spot. After four days, the reaction mixture is anaerobically filtered using a 0.2 µm syringe filter and transferred to a Schlenk flask. The solvent is removed in vacuo. Crystallization of the crude product using *n*-hexane/thf 2:3 at 8 °C results in crystal formation of piperidinium triflate as analyzed by SCXRD. To remove byproducts, column chromatography followed by crystallization as described for (A) was again performed. Yield: 7% (10 mg, 0.015 mmol).

^{1}H NMR (300 MHz, thf-d8): δ (ppm) = 7.06 (s, 2H, CH_2); 7.26–7.31 (m, 6H); 7.39–7.50 (m, 14H). ^{13}C NMR (300 MHz, thf-d8): δ (ppm) = 68.7 (CH_2); 126.5 ($CH_{arom.}$); 128.7 ($CH_{arom.}$); 129.7 ($CH_{arom.}$); 130.0 ($C_{quart.}$, phenyl); 130.2 ($CH_{arom.}$); 131.2 ($CH_{arom.}$); 132.0 ($CH_{arom.}$); 136.8 ($C_{quart.}$, phenyl); 150.4 ($C_{quart.}$, triazol); 183.7 ($C_{quart.}$, carbene); 212.8 ($C_{quart.}$, CO). DEPT-135 NMR (300 MHz, thf-d8): δ (ppm) = 68.7 (neg., CH_2); 126.5 (pos., $CH_{arom.}$); 128.7 (pos., $CH_{arom.}$); 129.7 (pos., $CH_{arom.}$); 130.2 (pos., $CH_{arom.}$); 131.2 (pos., $CH_{arom.}$); 132.0 (pos., $CH_{arom.}$). HSQC NMR (300 MHz, thf-d8): δ (ppm) = 7.06 and 68.7 (^{1}H, CH_2 and ^{13}C, CH_2); 7.30 and 128.7 (^{1}H, $CH_{arom.}$ And ^{13}C, $CH_{arom.}$); 7.30 and 129.7 (^{1}H, $CH_{arom.}$ And ^{13}C, $CH_{arom.}$); 7.43 and 126.5 (^{1}H, $CH_{arom.}$ And ^{13}C, $CH_{arom.}$); 7.43 and 130.2 (^{1}H, $CH_{arom.}$ And ^{13}C, $CH_{arom.}$), 7.43 and 131.2 (^{1}H, $CH_{arom.}$ And ^{13}C, $CH_{arom.}$), 7.43 and 132.0 (^{1}H, $CH_{arom.}$ And ^{13}C, $CH_{arom.}$). Rf-value (*n*-hexane/thf: 2/3): 0.9. IR (KBr), ν (cm^{-1}) = 3042 ($CH_{arom.}$), 1990 ($C{\equiv}O_{stretch}$),1864 ($C{\equiv}O_{stretch}$), 1810 ($C{\equiv}O_{stretch}$), 1696 ($C{=}N_{stretch}$), 1485-1428 (C=C), 1296-1022 ($CH_{arom., in\text{-}plane}$), 765 ($CH_{arom., out\text{-}of\text{-}plane}$).

4. Conclusions

The chelating bistriazolylidene MIC ligand (bta) employed in this study exhibits superior donor properties as confirmed by structural, spectroscopic and electrochemical investigations. The obtained molecular structures of precursor, ligand and complex facilitate a detailed insight into the structure of the ligand before and after coordination, and the rather dramatic requisite geometric reorganization to reach a structure optimal for chelating coordination was observed. The CO ligands of $[Mo(CO)_4(bta)]$ (**3**) are ideal reporter groups for the richness of the metal's electron density and thus provided a direct insight into the donor strength of the MIC ligand. The IR spectroscopic comparison with different related and unrelated mostly bidentate ligands highlights the notable donor capability of bta, which was confirmed by the relatively low oxidation potential found in the electrochemical experiment. All results re-emphasize that bta-type ligands constitute very promising (co-)ligands for the design of catalysts capable of small molecule activation. This shall be further investigated in future studies.

Supplementary Materials: The following supporting information can be downloaded at: https://www.mdpi.com/article/10.3390/inorganics10110216/s1, Figure S1: Structural comparison of (**1**) and (**1**)H^+; Figure S2: Structure of piperidinium triflate; Figure S3: Ligands used for comparison; Figure S4: Intermolecular hydrogen bonds in (**3**) and $[Mo(CO)_4(bipy)]$; Figure S5: ^{1}H NMR of 1,5-Diphenyl-1*H*-1,2,3-triazole (**1**); Figure S6: ^{13}C NMR of 1,5-Diphenyl-1*H*-1,2,3-triazole (**1**); Figure S7: ^{135}DEPT NMR of 1,5-Diphenyl-1*H* -1,2,3-triazole (**1**); Figure S8: IR spectrum of 1,5-Diphenyl-1*H*-1,2,3-triazole (**1**); Figure S9: ^{1}H NMR of 3,3′-Methylenebis(1,5-diphenyl-1*H*-1,2,3-triazol-3-ium) triflate (**2**); Figure S10: ^{13}C NMR of 3,3′-Methylenebis(1,5-diphenyl-1*H*-1,2,3-triazol-3-ium) triflate (**2**); Figure S11: ^{135}DEPT NMR of 3,3′-Methylenebis(1,5-diphenyl-1*H*-1,2,3-triazol-3-ium) triflate (**2**); Figure S12: IR spectrum of 3,3′-Methylenebis(1,5-diphenyl-1*H*-1,2,3-triazol-3-ium) triflate (**2**); Figure S13: ^{1}H NMR of $[Mo(CO)_4(bta)]$ (**3**); Figure S14: ^{13}C NMR of $[Mo(CO)_4(bta)]$ (**3**); Figure S15:

^{135}DEPT NMR of [Mo(CO)$_4$(bta)] (**3**); Figure S16: HSQC NMR of [Mo(CO)$_4$(bta)] (**3**); Figure S17: IR spectrum of [Mo(CO)$_4$(bta)] (**3**); Figure S18: Calculated frequencies and overlayed sum of gauss functions for [Mo(CO)4(bta)] (**3**); Figure S19: HOMO and LUMO of [Mo(CO)$_4$(bta)] (**3**); Table S1: More selected bond distances and angles of **1**, **2** and **3**; Table S2: Crystal data and structure refinement for 1,5-diphenyl-1*H*-1,2,3-triazole (**1**), Table S3: Crystal data and structure refinement for 3,3′-methylenebis(1,5-diphenyl-1*H*-1,2,3-triazol-3-ium) triflate (**2**); Table S4: Crystal data and structure refinement for [Mo(CO)$_4$(bta)] (**3**).

Author Contributions: Experimental investigation: B.J.E., P.S. and C.F.; formal analysis: B.J.E. and P.S.; additional investigation, validation: S.P.; writing—original draft preparation: B.J.E. and S.P.; DFT calculations: C.F.; crystallography: B.J.E. and C.S.; project administration: B.J.E., C.S. and C.F.; conceptualization: B.J.E. and C.S.; writing—review and editing, resources: C.S. All authors have read and agreed to the published version of the manuscript.

Funding: B.J.E. thanks the Deutsche Bundesstiftung Umwelt (DBU, AZ 20018/561) for his PhD-fellowship. C.S. and B.J.E. gratefully acknowledge generous financial support from the DFG (SCHU 1480/4-1).

Data Availability Statement: Not applicable.

Acknowledgments: The authors thank Gabriele Thede, Marlen Redies and Ashwani Bandaru for supporting this work with numerous NMR and CHNS service measurements.

Conflicts of Interest: The authors declare no conflict of interest.

References

1. Rostovtsev, V.V.; Green, L.G.; Fokin, V.V.; Sharpless, K.B. A Stepwise Huisgen Cycloaddition Process: Copper(I)-Catalyzed Regioselective "Ligation" of Azides and Terminal Alkynes. *Angew. Chem. Int. Ed.* **2002**, *41*, 2596–2599. [CrossRef]
2. Tornoe, C.W.; Christensen, C.; Meldal, M. Peptidotriazoles on solid phase: [1,2,3]-triazoles by regiospecific copper(i)-catalyzed 1,3-dipolar cycloadditions of terminal alkynes to azides. *J. Org. Chem.* **2002**, *67*, 3057–3064. [CrossRef] [PubMed]
3. Agard, N.J.; Baskin, J.M.; Prescher, J.A.; Lo, A.; Bertozzi, C.R. A comparative study of bioorthogonal reactions with azides. *ACS Chem. Biol.* **2006**, *1*, 644–648. [CrossRef]
4. Huisgen, R.; Knorr, R.; Möbius, L.; Szeimies, G. 1.3-Dipolare Cycloadditionen, XXIII. Einige Beobachtungen zur Addition organischer Azide an CC-Dreifachbindungen. *Chem. Ber.* **2006**, *98*, 4014–4021. [CrossRef]
5. Kwok, S.W.; Fotsing, J.R.; Fraser, R.J.; Rodionov, V.O.; Fokin, V.V. Transition-metal-free catalytic synthesis of 1,5-diaryl-1,2,3-triazoles. *Org. Lett.* **2010**, *12*, 4217–4219. [CrossRef]
6. Boren, B.C.; Narayan, S.; Rasmussen, L.K.; Zhang, L.; Zhao, H.; Lin, Z.; Jia, G.; Fokin, V.V. Ruthenium-catalyzed azide-alkyne cycloaddition: Scope and mechanism. *J. Am. Chem. Soc.* **2008**, *130*, 8923–8930. [CrossRef]
7. Huisgen, R.; Szeimies, G.; Möbius, L. 1.3-Dipolare Cycloadditionen, XXXII. Kinetik der Additionen organischer Azide an CC-Mehrfachbindungen. *Chem. Ber.* **2006**, *100*, 2494–2507. [CrossRef]
8. Schulze, B.; Schubert, U.S. Beyond click chemistry—supramolecular interactions of 1,2,3-triazoles. *Chem. Soc. Rev.* **2014**, *43*, 2522. [CrossRef] [PubMed]
9. Mathew, P.; Neels, A.; Albrecht, M. 1,2,3-Triazolylidenes as versatile abnormal carbene ligands for late transition metals. *J. Am. Chem. Soc.* **2008**, *130*, 13534–13535. [CrossRef]
10. Maity, R.; Sarkar, B. Chemistry of Compounds Based on 1,2,3-Triazolylidene-Type Mesoionic Carbenes. *JACS Au* **2022**, *2*, 22–57. [CrossRef]
11. Suntrup, L.; Hohloch, S.; Sarkar, B. Expanding the Scope of Chelating Triazolylidenes: Mesoionic Carbenes from the 1,5-Click-Regioisomer and Catalytic Synthesis of Secondary Amines from Nitroarenes. *Chem. Eur. J.* **2016**, *22*, 18009–18018. [CrossRef] [PubMed]
12. Arduengo, A.J.; Harlow, R.L.; Kline, M. A Stable Crystalline Carbene. *J. Am. Chem. Soc.* **1991**, *113*, 361–363. [CrossRef]
13. Hettmanczyk, L.; Manck, S.; Hoyer, C.; Hohloch, S.; Sarkar, B. Heterobimetallic complexes with redox-active mesoionic carbenes as metalloligands: Electrochemical properties, electronic structures and catalysis. *Chem. Commun.* **2015**, *51*, 10949–10952. [CrossRef] [PubMed]
14. Hettmanczyk, L.; Suntrup, L.; Klenk, S.; Hoyer, C.; Sarkar, B. Heteromultimetallic Complexes with Redox-Active Mesoionic Carbenes: Control of Donor Properties and Redox-Induced Catalysis. *Chem. Eur. J.* **2017**, *23*, 576–585. [CrossRef]
15. Vanicek, S.; Podewitz, M.; Stubbe, J.; Schulze, D.; Kopacka, H.; Wurst, K.; Muller, T.; Lippmann, P.; Haslinger, S.; Schottenberger, H., et al. Highly Electrophilic, Catalytically Active and Redox-Responsive Cobaltoceniumyl and Ferrocenyl Triazolylidene Coinage Metal Complexes. *Chemistry* **2018**, *24*, 3742–3753. [CrossRef]
16. Woods, J.A.; Lalrempuia, R.; Petronilho, A.; McDaniel, N.D.; Müller-Bunz, H.; Albrecht, M.; Bernhard, S. Carbene iridium complexes for efficient water oxidation: Scope and mechanistic insights. *Energy Environ. Sci.* **2014**, *7*, 2316–2328. [CrossRef]

17. van der Meer, M.; Glais, E.; Siewert, I.; Sarkar, B. Electrocatalytic Dihydrogen Production with a Robust Mesoionic Pyridylcarbene Cobalt Catalyst. *Angew. Chem. Int. Ed.* **2015**, *54*, 13792–13795. [CrossRef]
18. Suntrup, L.; Stein, F.; Klein, J.; Wilting, A.; Parlane, F.G.L.; Brown, C.M.; Fiedler, J.; Berlinguette, C.P.; Siewert, I.; Sarkar, B. Rhenium Complexes of Pyridyl-Mesoionic Carbenes: Photochemical Properties and Electrocatalytic CO_2 Reduction. *Inorg. Chem.* **2020**, *59*, 4215–4227. [CrossRef] [PubMed]
19. Kleinhans, G.; Guisado-Barrios, G.; Liles, D.C.; Bertrand, G.; Bezuidenhout, D.I. A rhodium(I)-oxygen adduct as a selective catalyst for one-pot sequential alkyne dimerization-hydrothiolation tandem reactions. *Chem. Commun.* **2016**, *52*, 3504–3507. [CrossRef]
20. Baschieri, A.; Monti, F.; Matteucci, E.; Mazzanti, A.; Barbieri, A.; Armaroli, N.; Sambri, L. A Mesoionic Carbene as Neutral Ligand for Phosphorescent Cationic Ir(III) Complexes. *Inorg. Chem.* **2016**, *55*, 7912–7919. [CrossRef]
21. Chabera, P.; Liu, Y.; Prakash, O.; Thyrhaug, E.; Nahhas, A.E.; Honarfar, A.; Essen, S.; Fredin, L.A.; Harlang, T.C.; Kjaer, K.S.; et al. A low-spin Fe(III) complex with 100-ps ligand-to-metal charge transfer photoluminescence. *Nature* **2017**, *543*, 695–699. [CrossRef] [PubMed]
22. Hettmanczyk, L.; Spall, S.J.P.; Klenk, S.; van der Meer, M.; Hohloch, S.; Weinstein, J.A.; Sarkar, B. Structural, Electrochemical, and Photochemical Properties of Mono- and Digold(I) Complexes Containing Mesoionic Carbenes. *Eur. J. Inorg. Chem.* **2017**, *2017*, 2112–2121. [CrossRef]
23. Matteucci, E.; Monti, F.; Mazzoni, R.; Baschieri, A.; Bizzarri, C.; Sambri, L. Click-Derived Triazolylidenes as Chelating Ligands: Achievement of a Neutral and Luminescent Iridium(III)-Triazolide Complex. *Inorg. Chem.* **2018**, *57*, 11673–11686. [CrossRef] [PubMed]
24. Sarkar, B.; Suntrup, L. Illuminating Iron: Mesoionic Carbenes as Privileged Ligands in Photochemistry. *Angew. Chem. Int. Ed.* **2017**, *56*, 8938–8940. [CrossRef] [PubMed]
25. Vivancos, A.; Segarra, C.; Albrecht, M. Mesoionic and Related Less Heteroatom-Stabilized N-Heterocyclic Carbene Complexes: Synthesis, Catalysis, and Other Applications. *Chem. Rev.* **2018**, *118*, 9493–9586. [CrossRef] [PubMed]
26. Guisado-Barrios, G.; Soleilhavoup, M.; Bertrand, G. 1*H*-1,2,3-Triazol-5-ylidenes: Readily Available Mesoionic Carbenes. *Acc. Chem. Res.* **2018**, *51*, 3236–3244. [CrossRef]
27. Guisado-Barrios, G.; Bouffard, J.; Donnadieu, B.; Bertrand, G. Bis(1,2,3-triazol-5-ylidenes) (i-bitz) as Stable 1,4-Bidentate Ligands Based on Mesoionic Carbenes (MICs). *Organometallics* **2011**, *30*, 6017–6021. [CrossRef]
28. Pinto, M.F.; Olivares, M.; Vivancos, Á.; Guisado-Barrios, G.; Albrecht, M.; Royo, B. (Di)triazolylidene manganese complexes in catalytic oxidation of alcohols to ketones and aldehydes. *Catal. Sci. Technol.* **2019**, *9*, 2421–2425. [CrossRef]
29. Friaes, S.; Realista, S.; Gomes, C.S.B.; Martinho, P.N.; Veiros, L.F.; Albrecht, M.; Royo, B. Manganese complexes with chelating and bridging di-triazolylidene ligands: Synthesis and reactivity. *Dalton Trans.* **2021**, *50*, 5911–5920. [CrossRef]
30. Suntrup, L.; Klenk, S.; Klein, J.; Sobottka, S.; Sarkar, B. Gauging Donor/Acceptor Properties and Redox Stability of Chelating Click-Derived Triazoles and Triazolylidenes: A Case Study with Rhenium(I) Complexes. *Inorg. Chem.* **2017**, *56*, 5771–5783. [CrossRef]
31. Vivancos, Á.; Albrecht, M. Influence of the Linker Length and Coordination Mode of (Di)Triazolylidene Ligands on the Structure and Catalytic Transfer Hydrogenation Activity of Iridium(III) Centers. *Organometallics* **2017**, *36*, 1580–1590. [CrossRef]
32. Hohloch, S.; Suntrup, L.; Sarkar, B. Arene–Ruthenium(II) and −Iridium(III) Complexes with "Click"-Based Pyridyl-triazoles, Bis-triazoles, and Chelating Abnormal Carbenes: Applications in Catalytic Transfer Hydrogenation of Nitrobenzene. *Organometallics* **2013**, *32*, 7376–7385. [CrossRef]
33. Sluijter, S.N.; Elsevier, C.J. Synthesis and Reactivity of Heteroditopic Dicarbene Rhodium(I) and Iridium(I) Complexes Bearing Chelating 1,2,3-Triazolylidene–Imidazolylidene Ligands. *Organometallics* **2014**, *33*, 6389–6397. [CrossRef]
34. Bolje, A.; Kosmrlj, J. A selective approach to pyridine appended 1,2,3-triazolium salts. *Org. Lett.* **2013**, *15*, 5084–5087. [CrossRef] [PubMed]
35. Bernet, L.; Lalrempuia, R.; Ghattas, W.; Mueller-Bunz, H.; Vigara, L.; Llobet, A.; Albrecht, M. Tunable single-site ruthenium catalysts for efficient water oxidation. *Chem. Commun.* **2011**, *47*, 8058–8060. [CrossRef]
36. Delgado-Rebollo, M.; Canseco-Gonzalez, D.; Hollering, M.; Mueller-Bunz, H.; Albrecht, M. Synthesis and catalytic alcohol oxidation and ketone transfer hydrogenation activity of donor-functionalized mesoionic triazolylidene ruthenium(II) complexes. *Dalton Trans.* **2014**, *43*, 4462–4473. [CrossRef]
37. Suntrup, L.; Stein, F.; Hermann, G.; Kleoff, M.; Kuss-Petermann, M.; Klein, J.; Wenger, O.S.; Tremblay, J.C.; Sarkar, B. Influence of Mesoionic Carbenes on Electro- and Photoactive Ru and Os Complexes: A Combined (Spectro-)Electrochemical, Photochemical, and Computational Study. *Inorg. Chem.* **2018**, *57*, 13973–13984. [CrossRef]
38. Leigh, V.; Ghattas, W.; Lalrempuia, R.; Muller-Bunz, H.; Pryce, M.T.; Albrecht, M. Synthesis, photo-, and electrochemistry of ruthenium bis(bipyridine) complexes comprising a N-heterocyclic carbene ligand. *Inorg. Chem.* **2013**, *52*, 5395–5402. [CrossRef]
39. Stubbe, J.; Neuman, N.I.; McLellan, R.; Sommer, M.G.; Nossler, M.; Beerhues, J.; Mulvey, R.E.; Sarkar, B. Isomerization Reactions in Anionic Mesoionic Carbene-Borates and Control of Properties and Reactivities in the Resulting Co(II) Complexes through Agostic Interactions. *Angew. Chem. Int. Ed.* **2021**, *60*, 499–506. [CrossRef]
40. Suntrup, L.; Beerhues, J.; Etzold, O.; Sarkar, B. Copper(I) complexes bearing mesoionic carbene ligands: Influencing the activity in catalytic halo-click reactions. *Dalton Trans.* **2020**, *49*, 15504–15510. [CrossRef]

41. Hidai, M.; Tominari, K.; Uchida, Y. Preparation and properties of dinitrogen-molybdenum complexes. *J. Am. Chem. Soc.* **1972**, *94*, 110–114. [CrossRef]
42. Ohki, Y.; Aoyagi, K.; Seino, H. Synthesis and Protonation of N-Heterocyclic-Carbene-Supported Dinitrogen Complexes of Molybdenum(0). *Organometallics* **2015**, *34*, 3414–3420. [CrossRef]
43. Beerhues, J.; Aberhan, H.; Streit, T.-N.; Sarkar, B. Probing Electronic Properties of Triazolylidenes through Mesoionic Selones, Triazolium Salts, and Ir-Carbonyl-Triazolylidene Complexes. *Organometallics* **2020**, *39*, 4557–4564. [CrossRef]
44. Elvers, B.J.; Sawall, M.; Oberem, E.; Heckenberger, K.; Ludwig, R.; Neymeyr, K.; Schulzke, C.; Krewald, V.; Fischer, C. Towards operando IR- and UV-vis-Spectro-Electrochemistry: A Comprehensive Matrix Factorisation Study on Sensitive and Transient Molybdenum and Tungsten Mono-Dithiolene Complexes. *Chemistry-Methods* **2021**, *1*, 22–35. [CrossRef]
45. Beerhues, J.; Fauche, K.; Cisnetti, F.; Sarkar, B.; Gautier, A. A dicopper(I)-dimesoionic carbene complex as a click catalyst: Mechanistic implications. *Dalton Trans.* **2019**, *48*, 8931–8936. [CrossRef]
46. Hsu, M.-A.; Yeh, W.-Y.; Chiang, M.Y. Syntheses, characterization and structures of $CpFe(CO)(\mu\text{-}I)(\mu\text{-}dppm)M(CO)_4$ (M=Cr, Mo, W). *J. Organomet. Chem.* **1998**, *552*, 135–143. [CrossRef]
47. Darensbourg, D.J.; Kump, R.L. A convenient synthesis of *cis*-$Mo(CO)_4L_2$ derivatives (L = Group 5a ligand) and a qualitative study of their thermal reactivity toward ligand dissociation. *Inorg. Chem.* **1978**, *17*, 2680–2682. [CrossRef]
48. Wieland, S.; van Eldik, R. Mechanistic Study of the Substitution Behavior of Complexes of the Type M(CO),(THF) (M = Cr, Mo, W). *Organometallics* **1991**, *10*, 3110–3114. [CrossRef]
49. Elvers, B.J.; Schulzke, C.; Fischer, C. Photochemical Unmasking of 1,3-Dithiol-2-ones: An Alternative Route to Heteroleptic Dithiolene Complexes from Low-Valent Molybdenum and Tungsten Precursors. *Eur. J. Inorg. Chem.* **2019**, *2019*, 2796–2805. [CrossRef]
50. Herrmann, W.A. N-Heterocyclic Carbenes: A New Concept in Organometallic Catalysis. *Angew. Chem. Int. Ed.* **2002**, *41*, 1290–1309. [CrossRef]
51. Poulain, A.; Canseco-Gonzalez, D.; Hynes-Roche, R.; Müller-Bunz, H.; Schuster, O.; Stoeckli-Evans, H.; Neels, A.; Albrecht, M. Synthesis and Tunability of Abnormal 1,2,3-Triazolylidene Palladium and Rhodium Complexes. *Organometallics* **2011**, *30*, 1021–1029. [CrossRef]
52. Navarro, M.; Wang, S.; Müller-Bunz, H.; Redmond, G.; Farràs, P.; Albrecht, M. Triazolylidene Metal Complexes Tagged with a Bodipy Chromophore: Synthesis and Monitoring of Ligand Exchange Reactions. *Organometallics* **2017**, *36*, 1469–1478. [CrossRef]
53. Sureshbabu, B.; Ramkumar, V.; Sankararaman, S. Facile base-free in situ generation and palladation of mesoionic and normal N-heterocyclic carbenes at ambient conditions. *Dalton Trans.* **2014**, *43*, 10710–10712. [CrossRef]
54. Hettmanczyk, L.; Schmid, B.; Hohloch, S.; Sarkar, B. Palladium(ii)-Acetylacetonato Complexes with Mesoionic Carbenes: Synthesis, Structures and Their Application in the Suzuki-Miyaura Cross Coupling Reaction. *Molecules* **2016**, *21*. [CrossRef] [PubMed]
55. Hahn, F.E.; Jahnke, M.C. Heterocyclic carbenes: Synthesis and coordination chemistry. *Angew. Chem. Int. Ed.* **2008**, *47*, 3122–3172. [CrossRef] [PubMed]
56. Gao, L.; Liu, T.; Tao, X.; Huang, Y. 2,2,6,6-Tetramethylpiperidinium triflate (TMPT): A highly selective and self-separated catalyst for esterification. *Tetrahedron Lett.* **2016**, *57*, 4905–4909. [CrossRef]
57. Suntrup, L.; Kleoff, M.; Sarkar, B. Serendipitous discoveries of new coordination modes of the 1,5-regioisomer of 1,2,3-triazoles enroute to the attempted synthesis of a carbon-anchored tri-mesoionic carbene. *Dalton Trans.* **2018**, *47*, 7992–8002. [CrossRef] [PubMed]
58. Groom, C.R.; Bruno, I.J.; Lightfoot, M.P.; Ward, S.C. The Cambridge Structural Database. *Acta Crystallogr. B* **2016**, *72*, 171–179. [CrossRef]
59. Stein, F.; Kirsch, M.; Beerhues, J.; Albold, U.; Sarkar, B. Mono- and Di-Mesoionic Carbene-Boranes: Synthesis, Structures and Utility as Reducing Agents. *Eur. J. Inorg. Chem.* **2021**, *2021*, 2417–2424. [CrossRef]
60. Bouffard, J.; Keitz, B.K.; Tonner, R.; Lavallo, V.; Guisado-Barrios, G.; Frenking, G.; Grubbs, R.H.; Bertrand, G. Synthesis of Highly Stable 1,3-Diaryl-1H-1,2,3-triazol-5-ylidenes and their Applications in Ruthenium-Catalyzed Olefin Metathesis. *Organometallics* **2011**, *30*, 2617–2627. [CrossRef]
61. Arduengo, A.J. Looking for Stable Carbenes: The Difficulty in Starting Anew. *Acc. Chem. Res.* **1999**, *32*, 913–921. [CrossRef]
62. Burling, S.; Field, L.D.; Li, H.L.; Messerle, B.A.; Turner, P. Mononuclear Rhodium(I) Complexes with Chelating N-Heterocyclic Carbene Ligands − Catalytic Activity for Intramolecular Hydroamination. *Eur. J. Inorg. Chem.* **2003**, *2003*, 3179–3184. [CrossRef]
63. Dierkes, P.; van Leeuwen, P.W.N.M. The bite angle makes the difference: A practical ligand parameter for diphosphine ligands. *J. Chem. Soc., Dalton Trans.* 1530. [CrossRef]
64. Gradert, C.; Krahmer, J.; Sonnichsen, F.D.; Nather, C.; Tuczek, F. Small-Molecule Activation with Molybdenum(0) Complexes Supported by Mixed Imidazol-2-Ylidene/Phosphanyl Hybrid Ligands—Electronic and Structural Consequences of Substituting a Phosphane by a Carbene Group. *Eur. J. Inorg. Chem.* **2013**, *2013*, 3943–3955. [CrossRef]
65. Gradert, C.; Krahmer, J.; Sönnichsen, F.D.; Näther, C.; Tuczek, F. Molybdenum(0)–carbonyl complexes supported by mixed benzimidazol-2-ylidene/phosphine ligands: Influence of benzannulation on the donor properties of the NHC groups. *J. Organomet. Chem.* **2014**, *770*, 61–68. [CrossRef]

66. Lappert, M.F.; Pye, P.L.; McLaughlin, G.M. Carbene complexes. Part 9. Electron-rich olefin-derived carbene–molybdenum(0) and amidinium molybdate(0) complexes, and the crystal and molecular structure of *cis*-tetracarbonylbis(1,3-dimethylimidazolidin-2-ylidene)molybdenum(0), cis-[$Mo(CO)_4${$CN(Me)CH_2CH_2NMe$}$_2$]. *J. Chem. Soc., Dalton Trans.* **1977**, 1272–1282. [CrossRef]
67. Bens, T.; Boden, P.; Di Martino-Fumo, P.; Beerhues, J.; Albold, U.; Sobottka, S.; Neuman, N.I.; Gerhards, M.; Sarkar, B. Chromium(0) and Molydenum(0) Complexes with a Pyridyl-Mesoionic Carbene Ligand: Structural, (Spectro)electrochemical, Photochemical, and Theoretical Investigations. *Inorg. Chem.* **2020**, *59*, 15504–15513. [CrossRef]
68. Maitra, K.; Nelson, J.H. Formation of 1,2-bis (diphenylphosphino)ethane, dppe, from two coordinated diphenylvinylphosphine (DPVP) ligands crystal structures of cis- and trans-$(DPVP)_2Mo(CO)_4$ and $(dppe)M(CO)_4$ (M=Cr, Mo). *Polyhedron* **1998**, *18*, 203–210. [CrossRef]
69. Braga, S.S.; Coelho, A.C.; Gonçalves, I.S.; Almeida Paz, F.A. (2,2′-Bipyridine)tetracarbonylmolybdenum(0). *Acta Crystallogr. E: Crystallogr. Commun.* **2007**, *63*, m780–m782. [CrossRef]
70. Öfele, K.; Herrmann, W.A.; Mihalios, D.; Elison, M.; Herdtweck, E.; Priermeier, T.; Kiprof, P. Heterocyclische Carbene IV. Metallkomplexe mit heterocyclischen Carben-Liganden: Synthese, Struktur, Strukturdynamik. *J. Organomet. Chem.* **1995**, *498*, 1–14. [CrossRef]
71. Clark, M.L.; Grice, K.A.; Moore, C.E.; Rheingold, A.L.; Kubiak, C.P. Electrocatalytic CO_2 reduction by $M(bpy\text{-}R)(CO)_4$ (M = Mo, W; R = H, *t*Bu) complexes. Electrochemical, spectroscopic, and computational studies and comparison with group 7 catalysts. *Chem. Sci.* **2014**, *5*, 1894–1900. [CrossRef]
72. Macholdt, H.-T.; Elias, H. Ligand Substitution in Molybdenum(0) Carbonyl Complexes $Mo(CO)_5$(amine) and cis -$Mo(CO)_4(amine)_2$: Kinetics and High-Pressure Effects. *Inorg. Chem.* **1984**, *23*, 4315–4321. [CrossRef]
73. Bock, H.; tom Dieck, H. Metall(0)-Verbindungen mit nichtaromatischen Stickstoff-π-Systemen, VI. 1.4-Diaza-butadien-molybdäntetracarbonyle: Synthesen, Eigenschaften und Bindungsmodell. *Chem. Ber.* **1967**, *100*, 228–246. [CrossRef]
74. Öfele, K.; Roos, E.; Herberhold, M. Isomerisierungsreaktionen von cis- und trans-Dicarben-Komplexen des Typs $M(CO)_4L_2$ (M = Cr, Mo, W). *Z. Naturforsch. B* **1976**, *31*, 1070–1077. [CrossRef]
75. Heinze, J. Cyclic Voltammetry—"Electrochemical Spectroscopy". *Angew. Chem. Int. Ed.* **1984**, *23*, 831–847. [CrossRef]
76. Farrugia, L.J. WinGX and ORTEP for Windows: An update. *J. Appl. Crystallogr.* **2012**, *45*, 849–854. [CrossRef]
77. Sheldrick, G.M. SHELXT—Integrated space-group and crystal-structure determination. *Acta Cryst. A* **2015**, *71*, 3–8. [CrossRef]
78. Sheldrick, G.M. Crystal structure refinement with SHELXL. *Acta Crystallogr. C Struct. Chem.* **2015**, *71*, 3–8. [CrossRef]
79. Neese, F. The ORCA program system. *WIREs Comput. Mol. Sci.* **2011**, *2*, 73–78. [CrossRef]
80. Becke, A.D. Density-functional exchange-energy approximation with correct asymptotic behavior. *Phys. Rev. A Gen. Phys.* **1988**, *38*, 3098–3100. [CrossRef]
81. Perdew, J.P. Density-functional approximation for the correlation energy of the inhomogeneous electron gas. *Phys. Rev. B Condens. Matter* **1986**, *33*, 8822–8824. [CrossRef]
82. Neese, F. An improvement of the resolution of the identity approximation for the formation of the Coulomb matrix. *J. Comput. Chem.* **2003**, *24*, 1740–1747. [CrossRef] [PubMed]
83. Weigend, F.; Ahlrichs, R. Balanced basis sets of split valence, triple zeta valence and quadruple zeta valence quality for H to Rn: Design and assessment of accuracy. *Phys. Chem. Chem. Phys.* **2005**, *7*, 3297–3305. [CrossRef]
84. Andrae, D.; Häußermann, U.; Dolg, M.; Stoll, H.; Preuß, H. Energy-adjustedab initio pseudopotentials for the second and third row transition elements. *Theor. Chim. Acta* **1990**, *77*, 123–141. [CrossRef]
85. Weigend, F. Accurate Coulomb-fitting basis sets for H to Rn. *Phys. Chem. Chem. Phys.* **2006**, *8*, 1057–1065. [CrossRef] [PubMed]
86. Grimme, S.; Antony, J.; Ehrlich, S.; Krieg, H. A consistent and accurate ab initio parametrization of density functional dispersion correction (DFT-D) for the 94 elements H-Pu. *J. Chem. Phys.* **2010**, *132*, 154104. [CrossRef] [PubMed]